

PiG-Avatar: Hierarchical Neural-Field-Guided Gaussian Avatars

JULIAN KALTHEUNER, University of Bonn, Germany

JAN SPINDLER, University of Bonn, Germany

SINA KITZ, University of Bonn, Germany

PATRICK STOTKO, University of Bonn, Germany

REINHARD KLEIN, University of Bonn, Germany

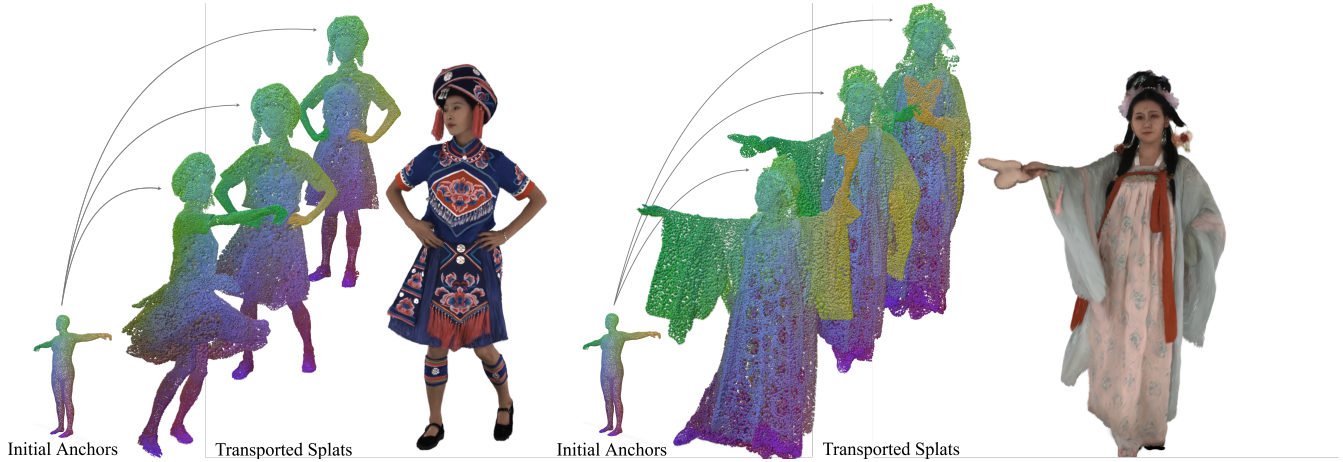


Fig. 1. We present *PiG-Avatar*, a Gaussian avatar method that decouples representation and deformation: the parametric model provides only kinematic transport, while a canonical neural field over learnable anchors is independent of template topology. Anchors self-organize in canonical space and, combined with time-conditioned neural features, produce temporally consistent posed splats, enabling complex, layered clothing and non-rigid motion.

Realistic animatable avatars of clothed humans are fundamental to virtual production, telepresence, and immersive experiences, yet reconstructing them from video remains challenging: clothing exhibits complex topology, layered geometry, and non-rigid dynamics that exceed what template-bound representations can faithfully capture. Existing Gaussian avatar methods typically parameterize geometry on a body-template surface, which entangles the avatar’s representation space with the template’s deformation space. Consequently, the template’s topology and sampling density impose a hard constraint on the representable geometry, precluding multi-layered garments, thick off-body clothing, and open-boundary surfaces unless explicit, case-specific mechanisms are introduced.

We present *PiG-Avatar*, which addresses this limitation by using the parametric body model solely for kinematic transport, while representing the avatar as Gaussians anchored in a volumetric canonical space governed by a continuous neural field. This decouples representation from template topology, avoiding the geometric constraints of surface-based parameterizations. Kinematic coherence is maintained through 3D barycentric anchor transport, which guides motion without constraining geometry and allows anchors to deviate freely from the template surface, yielding dense, stable temporal surface correspondences by construction. To make this unconstrained formulation tractable, we introduce dual-level spatially coherent optimization, combining Sobolev-preconditioned neural-field updates with a novel KNN-based preconditioning of canonical anchor geometry. Together, these mechanisms induce an emergent self-organization of anchor density:

anchors migrate toward regions of high curvature, appearance variation, and non-coherent motion without explicit heuristics. As a result, complex clothing geometry and layered surfaces emerge as natural, high-fidelity outputs. This single representation further supports hierarchical reconstruction across multiple levels of detail, with coarse-level supervision propagating to finer levels through the shared field and coupled anchor graph. On established benchmarks featuring subjects with complex clothing and challenging non-rigid motion, *PiG-Avatar* achieves state-of-the-art rendering quality, generalizes robustly to imperfect body model initialization, and renders in real time across all detail levels.

CCS Concepts: • **Computing methodologies** → **Reconstruction; Animation; Shape modeling; Rendering.**

Additional Key Words and Phrases: Gaussian Avatars, Neural Rendering, Level of Detail

1 Introduction

Realistic animatable human avatars are a key component of virtual production, telepresence, gaming, and immersive AR/VR experiences. A long-standing goal in computer graphics and vision is therefore to reconstruct digital humans from video in a form that is both visually faithful and controllable for animation. While remarkable progress has been made in recent years, modeling clothed humans remains challenging due to the complex geometry and motion of garments. Loose clothing, layered structures, wrinkles, and topology changes often violate the assumptions underlying standard articulated human representations.

Authors’ Contact Information: Julian Kaltheuner, University of Bonn, Germany, kaltheun@cs.uni-bonn.de; Jan Spindler, University of Bonn, Germany, jspindle@cs.uni-bonn.de; Sina Kitz, University of Bonn, Germany, kitz@cs.uni-bonn.de; Patrick Stotko, University of Bonn, Germany, stotko@cs.uni-bonn.de; Reinhard Klein, University of Bonn, Germany, rk@cs.uni-bonn.de.

Parametric body models such as SMPL [Loper et al. 2015], SMPL-X [Pavlakos et al. 2019], and related formulations [Ferguson et al. 2025; Xu et al. 2020] provide compact and highly controllable representations of human pose and shape. Because they establish a consistent articulated structure across time, they have become a common foundation for animatable avatar reconstruction. However, these models represent only minimally clothed bodies and cannot directly capture the geometry of real clothing. Earlier methods therefore augmented the body model with displacement surfaces, textures, or dynamic mesh refinements, but the resulting representations remained closely tied to the topology and resolution of the underlying template. Neural scene representations substantially increased the realism achievable for human reconstruction. Methods based on implicit fields and neural rendering [Mescheder et al. 2019; Mildenhall et al. 2020; Park et al. 2019] can represent highly detailed geometry and appearance while modeling complex non-rigid motion through learned deformation fields [Li et al. 2023b; Liu et al. 2021; Mu et al. 2023; Peng et al. 2021a,b; Weng et al. 2022]. More recently, 3D Gaussian Splatting (3DGS) [Kerbl et al. 2023] has enabled explicit scene representations with real-time rendering performance, making Gaussian-based approaches increasingly attractive for animatable avatars.

Most existing Gaussian avatar methods rely on the body template not only for articulation, but also as the parameterization domain of the representation itself. Gaussian primitives are commonly attached directly to the template mesh or parameterized in UV space defined on the body surface [Hu et al. 2024b,a; Jiang et al. 2025; Kocabas et al. 2024; Kwon et al. 2024; Pang et al. 2024; Qian et al. 2024]. This design provides stable animation and temporal consistency, but it also introduces a strong geometric bias: the structure of the representation inherits the topology, sampling density, and deformation behavior of the body model. Consequently, representable geometry is implicitly restricted to deformations of the template surface itself. In practice, this makes it difficult to faithfully represent garments that deviate substantially from the body surface, such as skirts, coats, layered clothing, or loose fabric with complex motion. Existing approaches often address these limitations through specialized clothing templates, additional deformation modules, or carefully initialized canonical meshes [Chen et al. 2025; Lee et al. 2025; Li et al. 2023a; Lin et al. 2024], increasing both modeling complexity and dependence on accurate priors.

In this work, we explore a different formulation. Instead of treating the body template as the geometric domain of the avatar representation, we use it only to provide kinematic guidance for motion. Our method, *PiG-Avatar*, represents the avatar using Gaussian anchors embedded directly in a canonical volumetric space, where geometry and appearance are modeled through a shared continuous neural field. The anchors are initialized with respect to a parametric articulated body model to obtain temporally consistent motion, but they are not constrained to remain on the template surface. As optimization proceeds, the anchors are free to reorganize in 3D space according to the observed geometry and motion of the subject, while the underlying body model parameters are refined to further strengthen motion alignment and stabilize this evolution. This joint refinement supports a more structured organization of the canonical representation without limiting anchors to the template surface, but

it also weakens the geometric regularization typically provided by the template. As a result, the canonical representation can become unstable or spatially incoherent, introducing a new optimization challenge: without the structural regularization imposed by a template surface, the representation must instead maintain coherence through learning alone. To address this, we enforce coherence at two complementary levels. First, updates of the shared canonical field are spatially smoothed through Sobolev preconditioning [Kalthener et al. 2026], encouraging coherent feature evolution in the latent representation. Second, we introduce a neighborhood-aware optimization scheme directly on the canonical anchor graph, coupling nearby anchors during geometric refinement. Together, these mechanisms encourage stable organization of the representation while preserving the flexibility needed to capture complex clothing geometry and non-rigid motion.

An additional advantage of our formulation is that the canonical representation remains temporally consistent by construction. Since anchors maintain stable identities over time while being transported through the articulated motion model, the method naturally produces dense temporal correspondences, as depicted in Figure 1, without requiring learned deformation tracking or post-processing alignment, directly enabling temporally consistent editing and transfer operations. Furthermore, the same canonical representation can be evaluated at multiple resolutions, allowing hierarchical avatar reconstruction within a single shared framework. We demonstrate that *PiG-Avatar* reconstructs high-fidelity animatable avatars with challenging clothing and motion while supporting real-time rendering. Experiments on established benchmarks show strong visual quality, robustness to imperfect body model initialization, and consistent performance across multiple levels of detail.

Our main contributions are:

- We identify the conflation of representation space and deformation space as the fundamental limitation of template-bound Gaussian avatar methods, and present *PiG-Avatar*, which achieves complete architectural decoupling: the parametric model provides only kinematic transport, while the canonical representation, a volumetric neural field over learnable anchor points, is independent of template topology. As a structural consequence, complex and layered clothing geometry emerges without case-specific provisions.
- We introduce a *3D barycentric anchor transport* mechanism that preserves kinematic coherence by consistently transporting Gaussian anchors through the articulated motion space, enabling stable and temporally consistent correspondences under deformation.
- We propose a *dual-level spatially coherent optimization* strategy that builds on Sobolev-preconditioned latent field updates and introduces a second preconditioning level on canonical anchor geometry via a fixed KNN graph. This design enforces spatial coherence simultaneously in the implicit field and explicit anchor positions, making topologically unconstrained canonical Gaussian optimization tractable without geometric regularization terms.

- We present a single unified hierarchical representation that is learned from a single model and supports progressive level-of-detail reconstruction and real-time rendering.

Code will be released upon publication.

2 Related Work

2.1 Implicit Neural Human Avatars

Neural rendering approaches have substantially advanced the reconstruction of animatable human avatars from images and videos. Many methods build upon parametric body models such as SMPL and SMPL-X [Loper et al. 2015; Pavlakos et al. 2019], which provide compact articulated priors for pose and shape and are commonly used to guide deformation between canonical and posed spaces.

A large body of work represents humans using implicit neural fields based on Neural Radiance Fields (NeRF). Early approaches such as Animatable NeRF [Peng et al. 2021a], A-NeRF [Su et al. 2021], and NeuMan [Jiang et al. 2022] learn canonical radiance fields that are animated through inverse skinning or pose-conditioned deformation fields. Subsequent works improve deformation modeling through structured local representations [Zheng et al. 2022a], bidirectional deformation mappings [Yu et al. 2023], or neural blend weight formulations [Peng et al. 2021a].

Several methods additionally introduce pose-aware latent representations to better model appearance variation. NeuralBody [Peng et al. 2021b] associates latent features with SMPL vertices, while NeuralActor [Liu et al. 2021] learns residual pose-dependent deformations on top of articulated priors. Later approaches, such as ActorsNeRF [Mu et al. 2023], PoseVocab [Li et al. 2023b], and TexVocab [Liu et al. 2024], further improve pose-conditioned appearance modeling via structured latent embeddings or texture vocabularies.

Another line of work focuses on canonical implicit surface representations instead of volumetric radiance fields. Methods such as SCANimate [Saito et al. 2021] and SNARF [Chen et al. 2021] improve generalization by learning deformation fields in canonical space. TAVA [Li et al. 2022] further relaxes reliance on predefined templates by learning canonical volumetric representations directly from observations. Generative approaches, such as AvatarGen [Zhang et al. 2022] and GetAvatar [Zhang et al. 2023], further explore latent canonical geometry spaces for controllable avatar synthesis. Despite their high visual fidelity, implicit neural avatar methods generally require computationally expensive volumetric rendering and dense sampling during both training and inference.

2.2 Gaussian-based Human Avatars

Explicit scene representations based on 3D Gaussian Splatting [Kerbl et al. 2023] have recently emerged as an efficient alternative to volumetric neural rendering. By representing scenes as collections of anisotropic Gaussian primitives, 3DGS enables high-quality rendering with substantially faster training and real-time inference, making it particularly attractive for animatable human avatars.

Most Gaussian avatar methods tightly couple primitives to a parametric human template. Surface-bound approaches such as 3DGS-Avatar [Qian et al. 2024], HUGS [Kocabas et al. 2024], GauHuman [Hu et al. 2024a], and SGIA [Zhao et al. 2025] attach Gaussians directly to template surfaces and animate them via linear blend

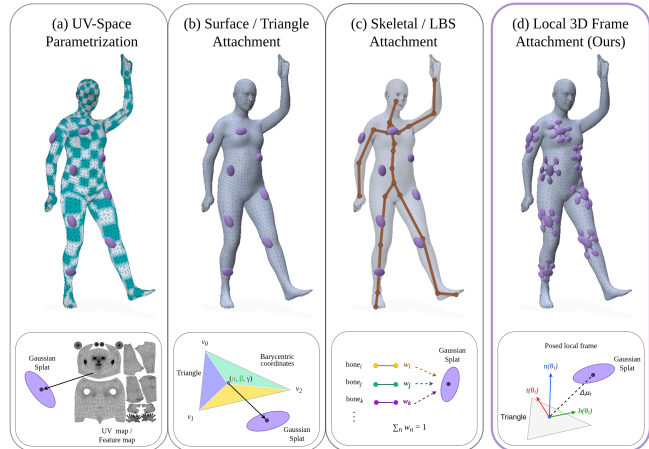


Fig. 2. Existing methods rely on UV maps, surface/triangle binding, or skeletal/LBS attachment, limiting deformation to the template. Our approach decouples anchors from template geometry, using canonical self-organization guided only by kinematic transport for flexible, non-rigid motion.

skinning. GART [Lei et al. 2024] learns articulated Gaussian templates initialized on a parametric surface and animated via learnable blend skinning, with limited freedom to deviate from the template geometry. Some methods additionally optimize skinning weights or pose refinements to improve deformation quality [Lei et al. 2024; Zhao et al. 2025]. Other approaches extend the underlying body representation itself to better capture clothing and secondary motion, for example through clothed templates or learned deformation modules [Chen et al. 2025; Lee et al. 2025].

A related direction parameterizes Gaussian attributes in the UV domain of the template surface. GaussianAvatar [Hu et al. 2024b], Animatable Gaussians [Li et al. 2024], and Relightable Gaussians [Li et al. 2023a] learn pose-dependent Gaussian properties via texture-like maps over the body template. Vid2Avatar-Pro [Guo et al. 2025] further introduces projective front/back maps and a pretrained universal prior for clothed avatar reconstruction. Other approaches employ CNN-based regressors in UV space to predict Gaussian attributes or geometry [Jiang et al. 2025; Kwon et al. 2024; Pang et al. 2024]. While these methods enable efficient and controllable animation, the learned representations remain tightly coupled to the template’s parameterization and deformation space.

2.3 Hybrid Mesh-Gaussian Representations

Several recent methods combine Gaussian splatting with explicit mesh representations to leverage the advantages of both paradigms. These hybrid approaches typically embed Gaussian primitives directly on mesh surfaces and learn neural models to predict pose-dependent appearance or local deformations.

GoMAvatar [Wen et al. 2024], RMAvatar [Peng et al. 2025], and SplattingAvatar [Shao et al. 2024] represent avatars using mesh-attached Gaussians combined with neural predictors for dynamic Gaussian attributes. Other works introduce layered or spatially distributed representations to better capture clothing deformation and local detail, including layered Gaussian avatars [Lin et al. 2024] and

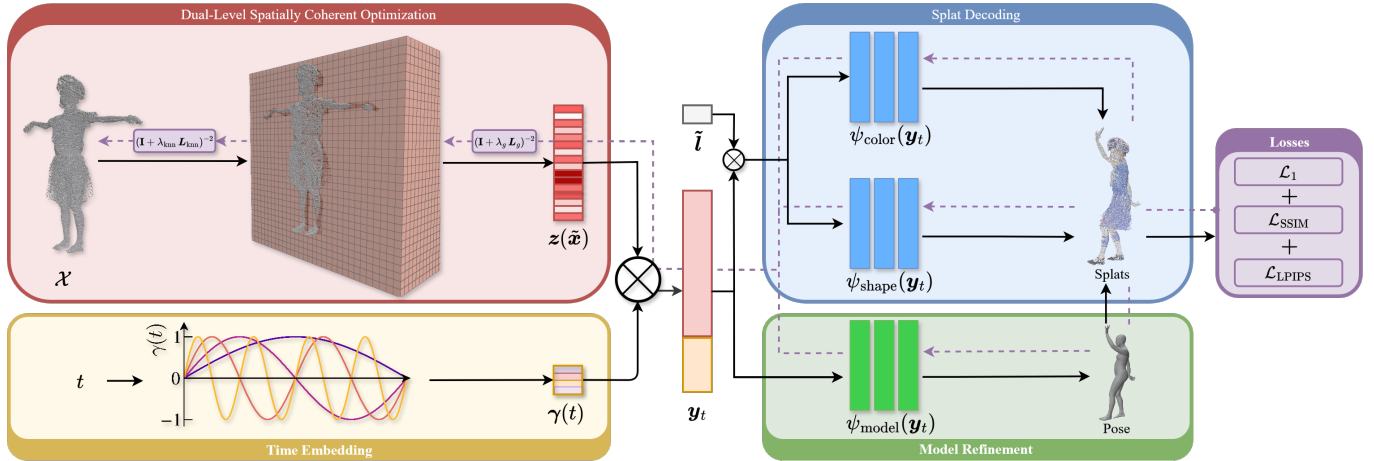


Fig. 3. Overview of PiG-Avatar. We learn a canonical, anchor-based Gaussian representation guided by a shared multi-resolution latent field. Conditioned on time and level of detail, lightweight decoders predict dynamic Gaussian attributes and refine a parametric proxy that transports anchors through time. This decoupled formulation enables stable geometry learning, articulated animation, and hierarchical reconstruction within a unified framework.

interpolated spatial MLPs [Zhan et al. 2025]. Additional approaches integrate Gaussian rendering with implicit geometry [Chen et al. 2024; Yuan et al. 2024], physics-based garment simulation [Lee et al. 2025], or relightable rendering [Choi et al. 2025].

Despite their strong rendering quality and efficiency, most existing Gaussian avatars remain fundamentally template-centered: Gaussian primitives are either attached to the template surface or directly parameterized in template space, thereby restricting the deformation to that of the model (see Figure 2). In contrast, our approach learns a spatially adaptive canonical Gaussian representation that is only kinematically guided by the articulated template, allowing more flexible modeling of loose clothing and complex non-rigid motion without requiring template-constrained geometry.

3 Method

Given a multi-view video sequence consisting of images $\{I_{c,t}\}$ captured from camera $c \in \{1, \dots, C\}$ at time $t \in \{1, \dots, T\}$, together with per-frame pose parameters obtained from a parametric body model such as SMPL-X, our goal is to reconstruct a high-fidelity animatable avatar that supports novel-view rendering and pose-driven animation. Our formulation decouples articulated motion from canonical geometric representation, as illustrated in Figure 3. We first use the body model purely as a kinematic prior to define temporally consistent articulation (Section 3.1), and introduce a transport mechanism that associates learnable Gaussian anchors with the articulated structure while allowing them to freely organize in canonical 3D space (Section 3.2). Subject geometry and appearance are represented by these anchors together with a shared neural field parameterized as a multi-resolution latent grid, which is optimized using a dual-level spatially coherent strategy that regularizes both the neural field and the canonical anchor geometry (Section 3.3). Finally, time-dependent geometry and appearance properties of the Gaussian primitives are decoded from the shared canonical representation using temporally conditioned decoders (Section 3.4).

Because all levels of detail share the same underlying representation, the model naturally supports hierarchical reconstruction and multi-resolution rendering within a unified framework.

3.1 Anchor-based Gaussian Avatar Model

We represent the avatar by a canonical set of 3D anchor points $\mathcal{X} = \{\mathbf{x}_i\}_{i=1}^N$ that define the support of the Gaussian representation. For each anchor \mathbf{x}_i , a spatial feature vector $\mathbf{z}(\mathbf{x}_i)$ is queried from a continuous neural field in canonical space, parameterized as a multi-resolution latent grid. This formulation decouples feature storage from anchor placement, such that representational capacity is not directly tied to the number or distribution of anchors. As a result, anchors can adaptively reorganize toward regions requiring increased geometric or appearance complexity, as depicted in Figure 4. Temporal variation is introduced only at the decoding stage by conditioning the queried canonical features on a time embedding. The canonical representation therefore remains shared across the entire sequence, while temporally conditioned MLP decoders predict dynamic Gaussian attributes $\{\boldsymbol{\mu}_{i,t}, \mathbf{q}_{i,t}, \mathbf{s}_{i,t}, \mathbf{o}_{i,t}, \mathbf{c}_{i,t}\}$ as well as refined parametric-model parameters $\{\boldsymbol{\beta}, \boldsymbol{\theta}_i\}$.

Nested Hierarchical Anchor Representation. To support reconstruction at multiple levels of detail (LOD) within a unified representation, we define a hierarchy of L nested anchor subsets. Starting from the full set of canonical anchors at the finest level, we recursively construct coarser levels by randomly subsampling anchors from the next finer level during initialization. This produces a nested hierarchy $\mathcal{X}_1 \subset \dots \subset \mathcal{X}_L = \mathcal{X}$, where each coarser level contains half as many anchors as the subsequent finer level, i.e., $|\mathcal{X}_{l-1}| = 0.5 |\mathcal{X}_l|$. The sampled indices are fixed after initialization and consistently define the active anchor subsets throughout training and inference.

This hierarchical construction couples optimization across levels of detail. All anchor subsets query the same canonical neural field, while the proposed dual-level spatially coherent optimization (see Section 3.3) propagates updates both through the shared

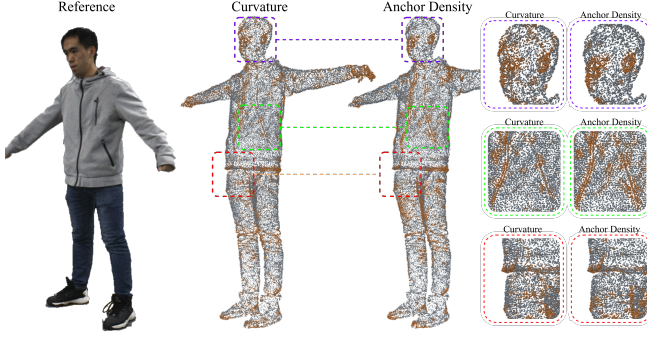


Fig. 4. Emergent anchor density from our spatially coherent optimization. Anchors concentrate in high-curvature regions, areas with strong appearance variation, and locations with complex local motion, while smoother, uniform regions remain sparse.

field representation and across neighboring anchors. Consequently, supervision applied at a coarse level also improves the canonical features used by finer levels. Moreover, anchors that are inactive in the current LOD continue to receive indirect geometric updates through neighborhood coupling, allowing finer LODs to remain consistent with the optimized coarse structure. In this way, all levels are jointly optimized within a single shared hierarchical representation.

Canonical Neural Field. We represent subject-specific canonical geometry and appearance using a shared neural field defined over canonical space. To parameterize this field, we adopt the preconditioned multi-resolution latent grid representation of Neu-PiG [Kaltheuner et al. 2026]. Concretely, the canonical volume is covered by G learnable regular grids with progressively increasing spatial resolution. Each grid stores a latent feature vector at every grid vertex. Given a normalized canonical query position $\tilde{\mathbf{x}}_i \in [-1, 1]^3$, we obtain a feature $\mathbf{z}_g(\tilde{\mathbf{x}}_i) \in \mathbb{R}^d$ from grid level g via trilinear interpolation. The final canonical feature descriptor is computed by averaging the interpolated features across all grid levels:

$$\mathbf{z}(\tilde{\mathbf{x}}_i) = \frac{1}{G} \sum_{g=1}^G \mathbf{z}_g(\tilde{\mathbf{x}}_i). \quad (1)$$

This multi-resolution parameterization enables the field to represent structure across different spatial scales while maintaining a fixed latent feature dimensionality.

3.2 3D Barycentric Anchor Transport

To enable temporally consistent articulation without restricting representational flexibility, we associate each canonical anchor point \mathbf{x}_i with the surface of a parametric body model (here, SMPL-X), which serves solely as a kinematic transport proxy throughout optimization. The body model does not define the final geometry of the avatar; instead, it provides structured motion guidance, while the Gaussian decoders (see Section 3.4) model local geometry and appearance around the transported anchors. Although we use SMPL-X in our experiments, the formulation is compatible with other articulated parametric geometry models.

Canonical Attachment. Anchor binding is performed directly in 3D using local surface frames rather than a 2D UV parameterization. Unlike UV binding, which requires a bijective map from the avatar surface and cannot capture multi-layer geometry or large off-surface displacements, 3D local-frame attachment provides kinematic guidance without imposing such constraints. Each canonical anchor is initialized from a reference surface point $\mathbf{x}_i^{\text{init}}$, sampled from the parametric model and stored as a fixed attachment. During optimization, the canonical anchor position \mathbf{x}_i remains fully learnable and may deviate from its initial surface location, while the attachment parameters remain fixed, preserving temporally consistent transport under articulated deformation and allowing anchors to reorganize freely in canonical space.

Pose-Dependent Transport. To transport an anchor \mathbf{x}_i into a posed frame at time t , we express its canonical offset relative to the reference surface point in the local canonical surface frame, rotate this offset into the posed local frame induced by the deforming proxy mesh, and add it to the posed surface position defined by the fixed barycentric attachment. Given pose parameters θ_t , we evaluate the posed reference surface point $\mathbf{x}_i^{\text{init}}(\theta_t)$ on the deformed proxy mesh, together with the corresponding posed local frame $(\mathbf{t}_i(\theta_t), \mathbf{b}_i(\theta_t), \mathbf{n}_i(\theta_t))$. The relative rotation between the canonical and posed local frames is defined as

$$\mathbf{R}_{i,t} = \begin{bmatrix} \mathbf{t}_i(\theta_t) & \mathbf{b}_i(\theta_t) & \mathbf{n}_i(\theta_t) \end{bmatrix} \begin{bmatrix} \mathbf{t}_i & \mathbf{b}_i & \mathbf{n}_i \end{bmatrix}^{\top}. \quad (2)$$

Using this rotation, the posed anchor position is computed as

$$\mathbf{x}_i(\theta_t) = \mathbf{x}_i^{\text{init}}(\theta_t) + \mathbf{R}_{i,t} (\mathbf{x}_i - \mathbf{x}_i^{\text{init}}). \quad (3)$$

This formulation keeps the barycentric attachment fixed while consistently rotating the canonical anchor offset with the evolving local surface frame under articulated deformation. As a result, anchors inherit temporally coherent articulated motion while remaining unconstrained by the topology and geometry of the proxy surface.

3.3 Dual-Level Spatially Coherent Optimization

Maintaining kinematic coherence for freely moving Gaussian anchors is essential to producing stable temporal correspondences. However, naive regularization can inadvertently restrict the model’s expressive capacity. To address this, we propose a dual-level spatially coherent preconditioning scheme, which combines Sobolev-preconditioned updates for the canonical neural field with a KNN-based preconditioning of the anchor positions. This design ensures both the latent field and the explicit anchor geometry evolve coherently in space while preserving the flexibility required to model complex, layered clothing and non-rigid deformations.

Grid-based Field Preconditioning. For each latent grid level g , the gradient with respect to the grid parameters \mathbf{z}_g is filtered using a resolution-dependent Laplacian operator before updating the grid:

$$\mathbf{z}_g \leftarrow \mathbf{z}_g - \eta_g (\mathbf{I} + \lambda_g \mathbf{L}_g)^{-2} \frac{\partial \mathcal{L}}{\partial \mathbf{z}_g}, \quad (4)$$

where η_g is the learning rate, λ_g controls the smoothing strength at level g , and \mathbf{L}_g encodes local neighborhood connectivity [Kaltheuner et al. 2026]. This Sobolev preconditioning acts as a low-pass filter on the latent updates, promoting smooth propagation of supervision

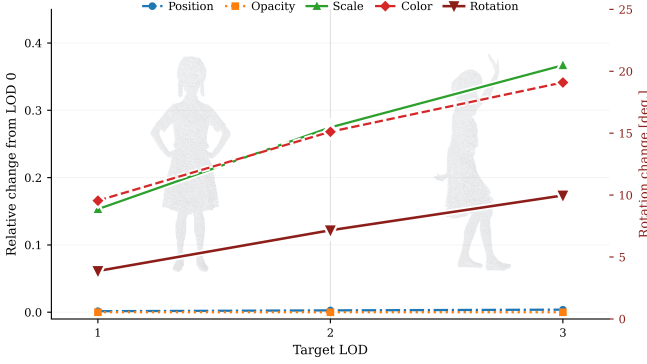


Fig. 5. Position and opacity remain stable across target LODs, whereas scale and color change substantially with increasing detail. Rotation varies more moderately, reaching about 10° at the highest target LOD. Overall, LOD conditioning primarily affects splat extent and appearance while preserving stable anchor positions across nested subsets.

across neighboring regions. As a result, nearby anchors querying the field obtain consistent descriptors, stabilizing the learning dynamics and improving temporal coherence.

KNN-based Anchor Preconditioning. In parallel, we regularize anchor positions using neighborhood-aware preconditioning defined on a fixed KNN graph in canonical space. Denoting the graph Laplacian as L_{knn} , anchor positions are updated as:

$$\mathbf{x} \leftarrow \mathbf{x} - \eta_{\text{knn}} (\mathbf{I} + \lambda_{\text{knn}} L_{\text{knn}})^{-2} \frac{\partial \mathcal{L}}{\partial \mathbf{x}}. \quad (5)$$

Here, η_{knn} is the anchor learning rate, and λ_{knn} governs the spatial coupling strength. These neighborhood relations are defined once in the canonical space and remain fixed throughout optimization, ensuring that nearby anchors remain coupled even after transport through the posed model. This coupling encourages local structural coherence, prevents anchor drift, and is particularly effective for modeling loose garments, folds, and other non-rigid motions.

Together, the Sobolev and KNN preconditionings induce an emergent self-organization of the anchors, allowing them to migrate naturally toward regions of high curvature, complex motion, or appearance variation without relying on hand-crafted heuristics. This emergent behavior improves spatial coverage of critical regions while preserving temporal consistency. Furthermore, this canonical coupling naturally supports hierarchical level-of-detail reconstruction: even inactive anchors in a given forward pass continue to receive indirect updates through their neighbors, reinforcing coherent structure across resolutions.

3.4 Time-Conditioned Gaussian Parameter Decoding

To model temporal variation, we combine the anchor-wise canonical descriptors with a temporal embedding and level-of-detail encoding.

For time, we adopt a Fourier feature embedding [Tancik et al. 2020] of the normalized timestep, $\tilde{t} = (t - 1)/(T - 1) \in [0, 1]$, mapping it to a multi-frequency sinusoidal representation:

$$\boldsymbol{\gamma}(t) = [\sin(\pi \nu_f \tilde{t}), \cos(\pi \nu_f \tilde{t})]_{f=1}^F, \quad (6)$$

where the exponentially increasing frequencies are $\nu_f = 2^{f-1}$. Following Neu-PiG [Kaltheuner et al. 2026], this embedding is used to modulate anchor-wise descriptors for time-dependent decoding, enabling fast and slow temporal variations to be represented within the same latent space.

Choosing F too small limits the temporal bandwidth and prevents accurate modeling of rapid pose- or appearance-dependent changes, while excessively large F allocates capacity to unnecessarily fine temporal variations. We therefore scale the number of frequency bands with the sequence length, setting $F = \lceil \log_2 T \rceil$. This produces a $2F$ -dimensional temporal descriptor suitable for both slow and fast temporal dynamics without fixing the embedding size a priori.

For hierarchical reconstruction, we further append the normalized level-of-detail variable $\tilde{l} = (l - 1)/(L - 1) \in [0, 1]$ to the decoder input. The final conditioning vector for an anchor i at timestep t and LOD l is:

$$\mathbf{y}_{i,t,l} = [\mathbf{z}(\tilde{\mathbf{x}}_i), \boldsymbol{\gamma}(t), \tilde{l}] \in \mathbb{R}^{d+2F+1}. \quad (7)$$

As also shown in Figure 5, this formulation ensures that temporal dynamics and multi-resolution effects are naturally incorporated into the anchor-wise decoding of both geometry and appearance.

3.4.1 Appearance Decoder. The view-dependent appearance of each anchor is predicted via a decoder Ψ_{color} mapping $\mathbf{y}_{i,t,l}$ to spherical harmonics coefficients:

$$\mathbf{c}_{i,t} = \Psi_{\text{color}}(\mathbf{y}_{i,t,l}). \quad (8)$$

For readability, we omit the explicit dependence of the predicted attributes on l in the notation; it is implicitly given through the decoder input $\mathbf{y}_{i,t,l}$.

We use separate MLP decoders for geometry and appearance to allow each to specialize to distinct spatial-frequency characteristics. In articulated human avatars, smooth surfaces like skin or clothing may still contain high-frequency details from textures, wrinkles, or fabric patterns, while regions with complex geometry, such as folds or facial features, can remain relatively uniform in color. By disentangling the decoding, each decoder focuses on the structural properties of its domain, improving representational capacity and enabling more accurate, high-fidelity reconstruction.

3.4.2 Shape Decoder. Geometric attributes of each Gaussian anchor are predicted by a dedicated decoder Ψ_{shape} :

$$\{\Delta \boldsymbol{\mu}_{i,t}, \Delta \mathbf{q}_{i,t}, \mathbf{s}_{i,t}, o_{i,t}\} = \Psi_{\text{shape}}(\mathbf{y}_{i,t,l}), \quad (9)$$

where $\Delta \boldsymbol{\mu}_{i,t} \in \mathbb{R}^3$ and $\Delta \mathbf{q}_{i,t} \in \mathbb{R}^4$ denote residual position and rotation offsets, $\mathbf{s}_{i,t} \in \mathbb{R}^3$ represents Gaussian scales, and $o_{i,t} \in \mathbb{R}$ encodes opacity. To ensure valid outputs, we adopt task-specific parameterizations: rotations are expressed as unit quaternions, scales are predicted in log-space, and opacities are constrained to $(0, 1)$.

The residual terms $\Delta \boldsymbol{\mu}_{i,t}$ and $\Delta \mathbf{q}_{i,t}$ capture local dynamic effects not explained by skeletal transport alone, such as clothing motion, folds, and subtle deformations. These residuals are combined with the pose-dependent transport described in Section 3.2 to compute final splat positions and orientations. Specifically, the final splat center for a posed anchor $\mathbf{x}_i(\boldsymbol{\theta}_t)$ from the parametric model is

$$\boldsymbol{\mu}_{i,t} = \mathbf{x}_i(\boldsymbol{\theta}_t) + \Delta \boldsymbol{\mu}_{i,t}, \quad (10)$$

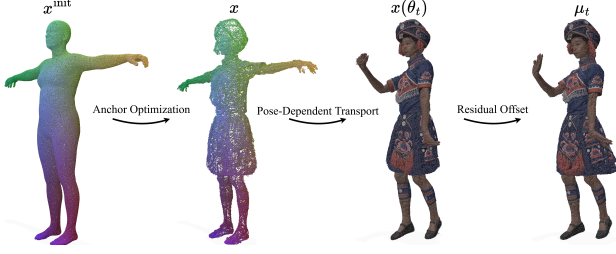


Fig. 6. Illustration of anchor transport through the deforming proxy mesh. Anchors first self-organize in canonical space, then follow kinematic motion with local offsets, producing the final Gaussian centers that track surface deformation consistently.

and the residual rotation, applied in the local posed frame, yields

$$\mathbf{q}_{i,t} = \mathbf{q}(\mathbf{R}_{i,t}) \Delta \mathbf{q}_{i,t}, \quad (11)$$

where $\mathbf{q}(\mathbf{R}_{i,t})$ converts the transported rotation $\mathbf{R}_{i,t}$ to quaternion space. This formulation preserves kinematic coherence while allowing anchors to deviate freely from the template, enabling the representation of complex layered and off-body clothing.

3.4.3 Global Parametric-Model Refinement. In addition to anchor-wise Gaussian attributes, we refine the underlying parametric body model to improve motion alignment and kinematic coherence. We predict residual updates to the model parameters using a global descriptor $\bar{\mathbf{z}}$ extracted from the canonical neural field. While Gaussian decoders operate on local anchor features, the parametric model encodes sequence-level structure and motion, motivating the use of a single global latent feature, which is obtained by averaging canonical latent features across all anchors:

$$\mathbf{y}_t = [\bar{\mathbf{z}}, \boldsymbol{\gamma}(t)], \quad \bar{\mathbf{z}} = \frac{1}{N} \sum_{i=1}^N \mathbf{z}(\tilde{\mathbf{x}}_i). \quad (12)$$

Unlike local decoders, this branch does not depend on the reconstruction level l , as it captures sequence-wide motion and shape information.

Given an initial parametric body model $(\boldsymbol{\beta}^{\text{init}}, \boldsymbol{\theta}_t^{\text{init}})$, we predict residual updates using a single MLP, Ψ_{model} :

$$\{\Delta \boldsymbol{\beta}_t, \Delta \boldsymbol{\theta}_t\} = \Psi_{\text{model}}(\mathbf{y}_t), \quad (13)$$

where $\Delta \boldsymbol{\beta}_t$ and $\Delta \boldsymbol{\theta}_t$ denote shape and pose corrections, respectively. Since the shape parameters $\boldsymbol{\beta}$ are time-invariant, we aggregate the predicted shape residuals across all timesteps during training to produce a single sequence-level update, $\Delta \boldsymbol{\beta}$. This averaging couples gradients temporally, producing a stable estimate of the overall shape. Pose corrections $\Delta \boldsymbol{\theta}_t$ remain timestep-specific, adapting to local motion, but are refined to preserve the articulated structure across the sequence. These globally-consistent corrections are important for properly disentangling anchor residuals and enabling the 3D barycentric anchor transport to establish stable, temporally consistent correspondences across frames.

The final model parameters are therefore

$$\boldsymbol{\beta} = \boldsymbol{\beta}^{\text{init}} + \Delta \boldsymbol{\beta}, \quad \boldsymbol{\theta}_t = \boldsymbol{\theta}_t^{\text{init}} + \Delta \boldsymbol{\theta}_t. \quad (14)$$

By predicting residuals relative to the initialization, rather than absolute values, this formulation stabilizes optimization and maintains the kinematic coherence used to guide anchor transport.

3.5 Optimization Objectives

We supervise reconstruction entirely in the image domain. Following MMLPHuman [Zhan et al. 2025], all losses are applied with silhouette-aware masking to suppress ambiguous boundary pixels. The overall objective is

$$\mathcal{L} = \lambda_1 \mathcal{L}_1 + \lambda_{\text{SSIM}} \mathcal{L}_{\text{SSIM}} + \lambda_{\text{LPIPS}} \mathcal{L}_{\text{LPIPS}}, \quad (15)$$

where \mathcal{L}_1 , $\mathcal{L}_{\text{SSIM}}$, and $\mathcal{L}_{\text{LPIPS}}$ denote pixel-wise L_1 , structural similarity, and perceptual losses, weighted by $\lambda_1 = 8$, $\lambda_{\text{SSIM}} = 2$, and $\lambda_{\text{LPIPS}} = 2$, respectively.

In contrast to many dynamic avatar methods, we do not employ explicit geometric or temporal regularization. Spatial coherence emerges naturally through the dual-level preconditioning scheme, while kinematic consistency and stable correspondences are maintained by the structured parametric model and 3D barycentric anchor transport, without additional temporal penalties.

For hierarchical reconstruction, a level-of-detail l is randomly sampled at each training iteration, and losses are computed only on the corresponding anchor subset \mathcal{X}_l , allowing coarse-level supervision to propagate to finer resolutions.

3.6 Implementation Details

We represent the avatar with a multi-resolution latent grid of $G = 6$ levels and $d = 16$ features per cell. The coarsest level has a resolution of 8^3 , and each finer level increases the resolution by a factor of 16 along each axis, reaching a finest resolution of 88^3 . The Gaussian splat representation is initialized with 100,000 anchors, without additional densification or pruning. View-dependent color is modeled using spherical harmonics of degree 3.

The model is optimized end-to-end with Adam [Kingma and Ba 2015] using the gsplat renderer. The parametric model network Ψ_{model} has three hidden layers of 32 units each, while the color and shape decoders, Ψ_{color} and Ψ_{shape} , each use five hidden layers of 512 units. Learning rates are 10^{-4} for Ψ_{model} and 10^{-3} for both decoders. For the latent grid, the base learning rate is 10^{-2} at the coarsest level and increases by $1.5\times$ per finer level; grid smoothness is scaled similarly, starting at $\lambda_g = 2$ and increasing by $1.25\times$ per level. Anchor positions use a learning rate of $2 \cdot 10^{-5}$ with $\lambda_{\text{knn}} = 8$.

Training is performed for 100,000 iterations, sampling 4 random views and 5 timesteps per iteration.

4 Evaluation

4.1 Datasets

We evaluate PiG-Avatar on THuman4 [Zheng et al. 2022b] and DNA-Rendering [Cheng et al. 2023], following established protocols to ensure fair comparison with prior work.

- *THuman4* contains dynamic performances of clothed human subjects captured with 24 calibrated RGB cameras at 30 FPS and a resolution of 1330×1150 . We evaluate on all three available subjects. For novel-view evaluation, 23 cameras are used for training while one camera is held out. For novel-pose evaluation, we

Table 1. Quantitative comparison on THuman4 across novel views, and novel poses. PSNR/SSIM \uparrow , LPIPS/FID \downarrow . Red and orange boxes indicate best and second-best results, respectively.

	Novel Views				Novel Poses				Splats
	PSNR \uparrow	SSIM \uparrow	LPIPS \downarrow	FID \downarrow	PSNR \uparrow	SSIM \uparrow	LPIPS \downarrow	FID \downarrow	
PoseVocab	24.90	0.965	0.038	109.72	24.06	0.958	0.043	105.29	-
AnimatableGS	28.25	0.973	0.036	56.83	27.38	0.961	0.043	42.49	361k
MMLPHuman	32.73	0.984	0.020	9.11	29.37	0.971	0.029	7.14	200k
Ours	32.57	0.982	0.023	8.07	28.08	0.967	0.033	10.95	100k

Table 2. Quantitative comparison on DNA across training views, novel views, and novel poses. PSNR/SSIM \uparrow , LPIPS/FID \downarrow . Red and orange boxes indicate best and second-best results, respectively.

	Novel Views				Novel Poses				Splats
	PSNR \uparrow	SSIM \uparrow	LPIPS \downarrow	FID \downarrow	PSNR \uparrow	SSIM \uparrow	LPIPS \downarrow	FID \downarrow	
PoseVocab	25.35	0.964	0.046	126.89	23.64	0.951	0.057	146.48	-
AnimatableGS	28.33	0.960	0.037	216.72	24.22	0.936	0.052	223.73	459k
MMLPHuman	31.83	0.981	0.027	13.18	25.58	0.951	0.048	36.13	200k
Ours	31.29	0.982	0.031	13.20	25.12	0.948	0.051	32.45	100k

train on the first 2000 timesteps and test on the remaining 500 timesteps.

- *DNA-Rendering* features multi-view sequences captured with 60 synchronized cameras and exhibits complex garments, loose clothing, and challenging non-rigid motion. We evaluate on the sequences 0165, 0166, and 0206. For novel-view evaluation, 48 cameras are used for training and 12 cameras are held out. For novel-pose evaluation, we train on 80% of each sequence and test on the remaining 20% of frames.

For novel-pose evaluation across both datasets, each query pose is mapped to the closest captured timestep in SMPL-X body-pose space. We compute the sum of per-joint geodesic distances in $SO(3)$ between joint rotations and select the nearest timestep as the reference clothing state.

4.2 Baselines and Evaluation Metrics

We compare PiG-Avatar against three state-of-the-art animatable human avatar methods: PoseVocab [Li et al. 2023b], AnimatableGS [Li et al. 2024], and MMLPHuman [Zhan et al. 2025].

To evaluate reconstruction fidelity and perceptual quality, we adopt PSNR, SSIM [Wang et al. 2004], LPIPS [Zhang et al. 2018], and FID [Heusel et al. 2017] as standard image-based metrics commonly used in human avatar rendering: PSNR and SSIM measure pixel-level reconstruction fidelity and structural similarity. LPIPS reflects perceptual similarity as judged by human observers. FID compares distributions of rendered and ground-truth images to assess perceptual realism.

4.3 Quantitative and Qualitative Evaluation

Tables 1 and 2 compare PiG-Avatar to recent avatar reconstruction methods on THuman4 and DNA-Rendering. Our method achieves competitive reconstruction quality while using a topology-decoupled

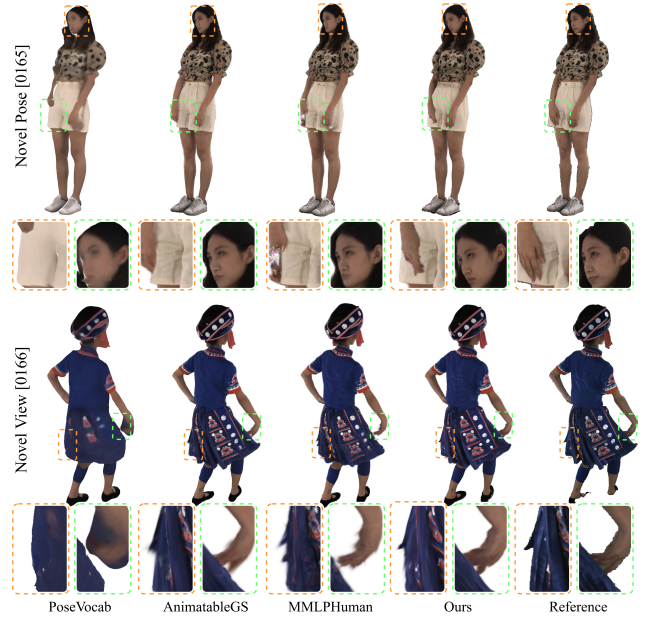


Fig. 7. Qualitative comparison on DNA for novel-pose synthesis (top, 0165) and novel-view synthesis (bottom, 0166). Zoom-ins highlight differences in facial detail, hand geometry, and clothing reconstruction.

canonical representation and, unlike the baselines, learns a single hierarchical model that supports multiple levels of detail. On THuman4, PiG-Avatar matches MMLPHuman in novel-view quality, attains the best FID, and uses only half as many splats. For novel-pose evaluation, it outperforms AnimatableGS and PoseVocab and remains close to MMLPHuman despite the reduced number of primitives. On DNA-Rendering, PiG-Avatar maintains competitive novel-view performance and achieves the best FID for novel poses, demonstrating strong perceptual consistency under challenging pose generalization. Qualitative results in Figure 7 show that PiG-Avatar preserves overall body shape, garment structure, and fine local appearance details in challenging regions such as faces, silhouettes, and textured clothing.

4.4 Level-of-Detail Evaluation

Table 3 evaluates the level-of-detail behavior of our shared hierarchical representation. Reconstruction quality remains stable across resolutions while memory usage and runtime scale proportionally with the number of active splats. Even the coarsest level with 12.5k splats achieves high-quality reconstruction and renders at 242 FPS, whereas the full 100k-splat representation further improves perceptual fidelity while maintaining real-time performance. Figure 8 illustrates the corresponding visual trade-off, with coarse LODs preserving the global avatar structure and appearance and finer levels recovering additional local details in both the splat distribution and renderings. These results demonstrate progressive real-time rendering from a single trained model without requiring separate fixed-resolution avatars.



Fig. 8. LOD comparison of our shared hierarchical representation, showing splat structure colored by base color and corresponding renderings. Zoom-ins highlight local geometry and appearance details across resolutions.

Table 3. Memory consumption and rendering performance (FPS) across levels of detail (LOD), evaluated on novel views on the THuman4D dataset on an NVIDIA RTX 5090 GPU. Red and orange boxes indicate best and second-best results, respectively.

LOD	Splats	PSNR \uparrow	SSIM \uparrow	LPIPS \downarrow	FID \downarrow	MB \downarrow	FPS \uparrow
1/4	12.5k	32.52	0.981	0.029	9.87	8.68	242
2/4	25k	32.63	0.981	0.027	8.99	9.73	159
3/4	50k	32.64	0.982	0.025	8.34	11.82	93
4/4	100k	32.57	0.982	0.023	8.07	16.02	52
1/1	100k	32.66	0.982	0.023	8.42	16.02	52

4.5 Ablation Studies

Our ablation study investigates the contribution of the main structural components of PiG-Avatar and analyzes its robustness to noise in the input SMPL-X parameters.

Structural Ablations. To evaluate the contribution of PiG-Avatar’s key structural components, we perform an ablation study in which individual elements are removed while all other settings remain unchanged, with results summarized in Table 4. We test the effect of fixing canonical anchors without refinement to assess the role of anchor mobility, removing per-timestep splat offsets $\Delta\mu_{i,t}$ to measure the impact of local dynamic adjustments, disabling dual-level preconditioning to examine its influence on spatially coherent canonical geometry and optimization stability, and replacing separate MLPs for splat shape and color with a single shared MLP to evaluate the benefit of decoupling geometry and appearance.

Removing the residual position offsets causes the largest performance drop, confirming that decoder-predicted local dynamics are the most critical component for modeling non-rigid clothing motion. Notably, even without anchor optimization, the model still achieves the second-best overall results, indicating that the preconditioned shared latent representation already provides a strong geometric prior when decoded by the MLPs. In contrast, removing dual-level preconditioning leads to clear degradation across all metrics, highlighting its importance for spatially coherent canonical geometry and stable optimization. Using a single splat MLP

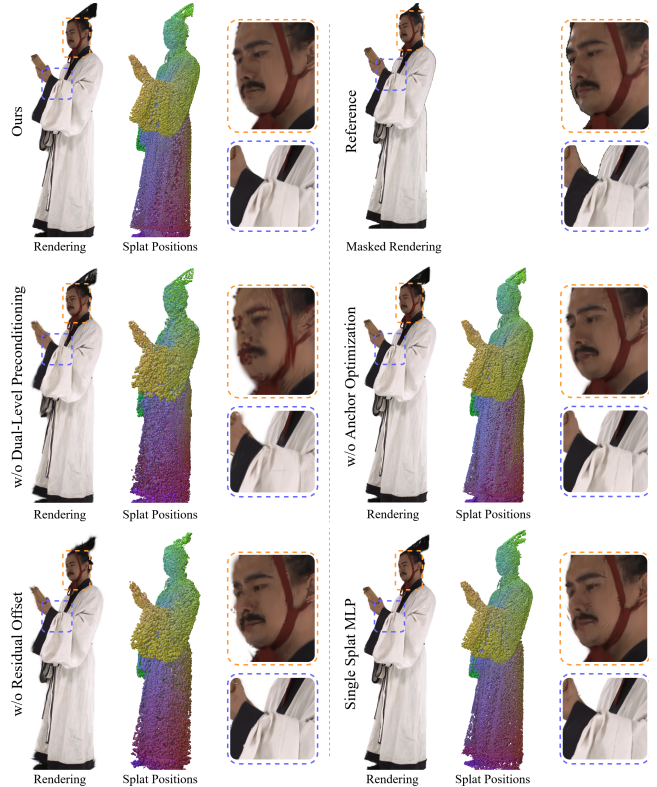


Fig. 9. Qualitative structural ablations on DNA. Compared to our full model, removing residual offsets, anchor optimization, dual-level preconditioning, or the disentangled shape/color decoders degrades local detail and splat organization, highlighted in the face and sleeve regions.

Table 4. Structural ablation study on DNA-dataset subject 0102, novel views. Red and orange boxes indicate best and second-best results, respectively.

	PSNR \uparrow	SSIM \uparrow	LPIPS \downarrow	FID \downarrow
w/o Dual-Level Preconditioning	28.17	0.977	0.054	24.54
w/o Anchor Optimization	28.45	0.981	0.047	13.50
w/o Residual Position Offsets	27.24	0.975	0.053	36.51
Single Splat MLP	28.29	0.977	0.054	24.54
Ours	28.61	0.981	0.046	12.66

also reduces performance, showing that disentangling shape and appearance remains beneficial.

Robustness to Noisy SMPL-X Parameters. To evaluate the robustness of our model-based formulation, we analyze how well the representation compensates for inaccuracies in the parametric body model, which in practical settings are often estimated by external pose reconstruction methods and may contain non-negligible errors. We simulate imperfect model estimates by perturbing the SMPL-X pose and shape parameters with additive zero-mean Gaussian noise

Table 5. Robustness to noisy SMPL-X parameters on DNA-Rendering subject 0012, evaluated on novel views. Increasing σ_{body} indicates stronger body pose perturbations. PiG-Avatar degrades gracefully under moderate noise, demonstrating robustness to imperfect parametric model initialization.

σ_{body}	PSNR \uparrow	SSIM \uparrow	LPIPS \downarrow	FID \downarrow
0 / 0°	29.33	0.977	0.030	18.07
0.1 / 5.7°	29.12	0.977	0.030	17.00
0.2 / 11.3°	28.67	0.976	0.031	17.84
0.25 / 14.3°	28.67	0.974	0.034	27.57

of increasing magnitude and use the perturbed parameters as input to the model decoder, while following the same training and evaluation protocol as in the main experiments.

Quantitative results in Table 5 show that performance degrades gracefully as the noise level increases, indicating that the learnable canonical anchors and residual splat offsets effectively compensate for moderate model inaccuracies. The canonical refinement corrects systematic shape deviations, and the residual dynamic offsets mitigate pose-dependent misalignments. Qualitative results in Figure 10 further illustrate that even under noticeable perturbations of the SMPL-X parameters, PiG-Avatar recovers accurate surface alignment and appearance, demonstrating strong robustness to realistic model estimation errors.

4.6 Limitations

For fine-grained articulated parts of the human body model, particularly the fingers in SMPL-X, the actual pose may only be partially recovered from the input estimate, as local learned deformations can also capture the apparent articulation. These structures are on a similar geometric scale as the local deformations, which makes full disentanglement challenging.

In addition, PiG-Avatar relies on persistent anchor-to-surface correspondences to transport canonical splats through the articulated model. While this generally ensures stable motion under typical deformations, it can be challenged when anchors become ambiguous due to sustained interactions between topdistant body parts. For example, if a subject holds their hands at their hips throughout the sequence, anchors on the hands and hips can become less distinguishable, potentially causing minor misalignment or artifacts.

Furthermore, because we do not perform anchor densification, the anchor resolution at some regions may be lower than ideal for representing very fine details.

5 Conclusion

We introduced PiG-Avatar, a method for reconstructing high-fidelity, animatable Gaussian avatars from multi-view video. By representing geometry in a canonical neural field and decoupling the avatar representation from the parametric body model, which is used solely for kinematic guidance, our approach avoids the geometric constraints of template-based methods. Canonical anchors sample the neural field and adapt their spatial distribution while maintaining temporal coherence, enabling stable optimization and dense, consistent surface correspondences. This design allows PiG-Avatar to accurately capture complex clothing, layered surfaces, and non-rigid motion

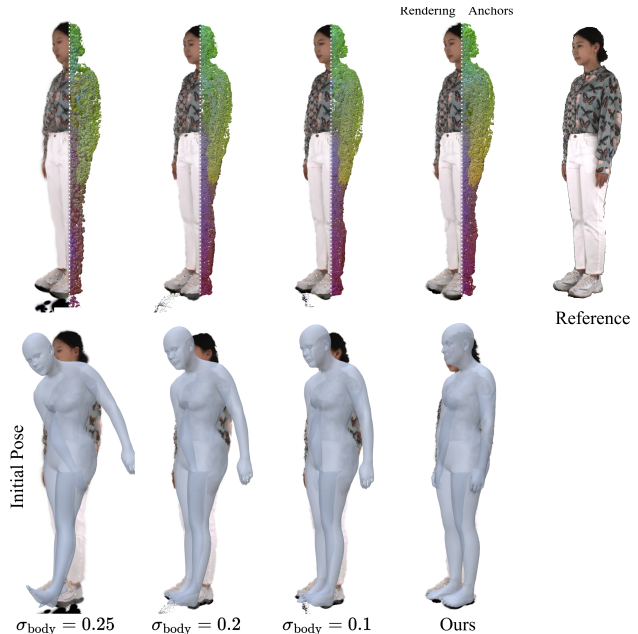


Fig. 10. Robustness to noisy SMPL-X parameters. Left: ground-truth image. Middle: noisy SMPL-X mesh overlay. Right: reconstruction produced by our method using the same noisy input. Despite significant perturbation of pose and shape parameters, our formulation corrects misalignments and recovers accurate geometry.

while remaining robust to imperfect body model initialization. Our experiments demonstrate competitive perceptual quality, real-time rendering at multiple levels of detail, and reliable generalization to challenging poses and novel views, highlighting the versatility and effectiveness of our hierarchical canonical Gaussian representation.

Acknowledgements

This work was supported by the European Regional Development Fund (ERDF) and the State of North Rhine-Westphalia as part of the operational program EFRE/JTF-Programm NRW 2021-2027. The project, titled “Gen-Avatar”, was funded under the NEXT.IN.NRW competition with the grant agreement No. EFRE-20801085.

Additionally, it has been funded by the Federal Ministry of Education and Research of Germany and the state of North-Rhine Westphalia as part of the Lamarr-Institute for Machine Learning and Artificial Intelligence and by the Federal Ministry of Education and Research under Grant No. 01IS22094A WEST-AI.

The work has also been funded by the Ministry of Culture and Science North Rhine-Westphalia under grant number PB22-063A (InVirtuo 4.0: Experimental Research in Virtual Environments), and by the state of North Rhine Westphalia as part of the Excellency Start-up Center.NRW (U-BO-GROW) under grant number 03ESCNW18B.

References

- Jianchuan Chen, Jingchuan Hu, Gaige Wang, Zhonghua Jiang, Tiansong Zhou, Zhiwen Chen, and Chengfei Lv. 2025. TaoAvatar: Real-Time Lifelike Full-Body Talking Avatars for Augmented Reality via 3D Gaussian Splatting. In *IEEE/CVF Conference on Computer Vision and Pattern Recognition (CVPR)*.

- Xu Chen, Yufeng Zheng, Michael J. Black, Otmar Hilliges, and Andreas Geiger. 2021. SNARF: Differentiable Forward Skinning for Animating Non-Rigid Neural Implicit Shapes. In *IEEE International Conference on Computer Vision (ICCV)*.
- Yushuo Chen, Zerong Zheng, Zhe Li, Chao Xu, and Yebin Liu. 2024. Meshavatar: Learning high-quality triangular human avatars from multi-view videos. In *European Conference on Computer Vision (ECCV)*.
- Wei Cheng, Ruixiang Chen, Siming Fan, Wanqi Yin, Keyu Chen, Zhongang Cai, Jingbo Wang, Yang Gao, Zhengming Yu, Zhengyu Lin, et al. 2023. Dna-rendering: A diverse neural actor repository for high-fidelity human-centric rendering. In *IEEE International Conference on Computer Vision (ICCV)*. 19982–19993.
- Seonghwa Choi, Moonkyeong Choi, Mingyu Jang, Jaekyung Kim, Jianfei Cai, Wen-Huang Cheng, and Sanghoon Lee. 2025. Relightable and Dynamic Gaussian Avatar Reconstruction from Monocular Video. In *ACM International Conference on Multimedia*.
- Aaron Ferguson, Ahmed AA Osman, Berta Bescos, Carsten Stoll, Chris Twigg, Christoph Lassner, David Otte, Eric Vignola, Fabian Prada, Federica Bogo, et al. 2025. Mhr: Momentum human rig. *arXiv preprint arXiv:2511.15586* (2025).
- Chen Guo, Junxuan Li, Yash Kant, Yaser Sheikh, Shunsuke Saito, and Chen Cao. 2025. Vid2avatar-pro: Authentic avatar from videos in the wild via universal prior. In *IEEE/CVF Conference on Computer Vision and Pattern Recognition (CVPR)*.
- Martin Heusel, Hubert Ramsauer, Thomas Unterthiner, Bernhard Nessler, and Sepp Hochreiter. 2017. GANs Trained by a Two Time-Scale Update Rule Converge to a Local Nash Equilibrium. *Advanced Neural Information Processing Systems (NeurIPS)* 30 (2017).
- Liangxiao Hu, Hongwen Zhang, Yuxiang Zhang, Boyao Zhou, Boning Liu, Shengping Zhang, and Liqiang Nie. 2024b. GaussianAvatar: Towards Realistic Human Avatar Modeling from a Single Video via Animatable 3D Gaussians. In *IEEE/CVF Conference on Computer Vision and Pattern Recognition (CVPR)*.
- Shoukang Hu, Tao Hu, and Ziwei Liu. 2024a. GauHuman: Articulated Gaussian Splatting from Monocular Human Videos. In *IEEE/CVF Conference on Computer Vision and Pattern Recognition (CVPR)*.
- Wei Jiang, Kwang Moo Yi, Golnoosh Samei, Oncel Tuzel, and Anurag Ranjan. 2022. Neuman: Neural human radiance field from a single video. In *European Conference on Computer Vision (ECCV)*.
- Yujiao Jiang, Qingmin Liao, Xiaoyu Li, Li Ma, Qi Zhang, Chaopeng Zhang, Zongqing Lu, and Ying Shan. 2025. Uv gaussians: Joint learning of mesh deformation and gaussian textures for human avatar modeling. *Knowledge-Based Systems* 320 (2025).
- Julian Kaltheuner, Hannah Dröge, Markus Plack, Patrick Stotko, and Reinhard Klein. 2026. Neu-PiG: Neural Preconditioned Grids for Fast Dynamic Surface Reconstruction on Long Sequences. In *IEEE/CVF Conference on Computer Vision and Pattern Recognition (CVPR)*.
- Bernhard Kerbl, Georgios Kopanas, Thomas Leimkühler, and George Drettakis. 2023. 3D Gaussian splatting for real-time radiance field rendering. *ACM Transactions on Graphics (TOG)* 42, 4 (2023).
- Diederik P Kingma and Jimmy Ba. 2015. Adam: A Method for Stochastic Optimization. In *International Conference on Learning Representations (ICLR)*.
- Muhammed Kocabas, Jen-Hao Rick Chang, James Gabriel, Oncel Tuzel, and Anurag Ranjan. 2024. HUGS: Human Gaussian Splats. In *IEEE/CVF Conference on Computer Vision and Pattern Recognition (CVPR)*.
- Youngjoong Kwon, Baole Fang, Yixing Lu, Haoye Dong, Cheng Zhang, Francisco Vicente Carrasco, Albert Mosella-Montoro, Jianjin Xu, Shingo Takagi, Daeil Kim, et al. 2024. Generalizable human gaussians for sparse view synthesis. In *European Conference on Computer Vision (ECCV)*.
- Changmin Lee, Jihyun Lee, and Tae-Kyun Kim. 2025. MPMAvatar: Learning 3D Gaussian Avatars with Accurate and Robust Physics-Based Dynamics. In *Advanced Neural Information Processing Systems (NeurIPS)*.
- Jiahui Lei, Yufu Wang, Georgios Pavlakos, Lingjie Liu, and Kostas Daniilidis. 2024. GART: Gaussian Articulated Template Models. In *IEEE/CVF Conference on Computer Vision and Pattern Recognition (CVPR)*.
- Ruilong Li, Julian Tanke, Minh Vo, Michael Zollhöfer, Jürgen Gall, Angjoo Kanazawa, and Christoph Lassner. 2022. Tava: Template-free animatable volumetric actors. In *European Conference on Computer Vision (ECCV)*.
- Zhe Li, Yipeng Sun, Zerong Zheng, Lizhen Wang, Shengping Zhang, and Yebin Liu. 2023a. Animatable and relightable gaussians for high-fidelity human avatar modeling. *arXiv preprint arXiv:2311.16096* (2023).
- Zhe Li, Zerong Zheng, Yuxiao Liu, Boyao Zhou, and Yebin Liu. 2023b. Posevocab: Learning joint-structured pose embeddings for human avatar modeling. In *ACM SIGGRAPH Conference Papers*.
- Zhe Li, Zerong Zheng, Lizhen Wang, and Yebin Liu. 2024. Animatable gaussians: Learning pose-dependent gaussian maps for high-fidelity human avatar modeling. In *IEEE/CVF Conference on Computer Vision and Pattern Recognition (CVPR)*.
- Siyu Lin, Zhe Li, Zhaoqi Su, Zerong Zheng, Hongwen Zhang, and Yebin Liu. 2024. Layga: Layered gaussian avatars for animatable clothing transfer. In *ACM SIGGRAPH Conference Papers*.
- Lingjie Liu, Marc Habermann, Viktor Rudnev, Kripasindhu Sarkar, Jiatao Gu, and Christian Theobalt. 2021. Neural Actor: Neural Free-view Synthesis of Human Actors with Pose Control. *ACM Transactions on Graphics (TOG)* 40, 6 (2021).
- Yuxiao Liu, Zhe Li, Yebin Liu, and Haoqian Wang. 2024. TexVocab: Texture Vocabulary-conditioned Human Avatars. In *IEEE/CVF Conference on Computer Vision and Pattern Recognition (CVPR)*.
- Matthew Loper, Naureen Mahmood, Javier Romero, Gerard Pons-Moll, and Michael J Black. 2015. SMPL: A Skinned Multi-Person Linear Model. *ACM Transactions on Graphics (TOG)* 34, 6 (2015).
- Lars Mescheder, Michael Oechsle, Michael Niemeyer, Sebastian Nowozin, and Andreas Geiger. 2019. Occupancy Networks: Learning 3D Reconstruction in Function Space. In *IEEE/CVF Conference on Computer Vision and Pattern Recognition (CVPR)*.
- Ben Mildenhall, Pratul P Srinivasan, Matthew Tancik, Jonathan T Barron, Ravi Ramamoorthi, and Ren Ng. 2020. NeRF: Representing Scenes as Neural Radiance Fields for View Synthesis. In *European Conference on Computer Vision (ECCV)*.
- Jiteng Mu, Shen Sang, Nuno Vasconcelos, and Xiaolong Wang. 2023. ActorsNeRF: Animatable Few-shot Human Rendering with Generalizable NeRFs. In *IEEE International Conference on Computer Vision (ICCV)*.
- Haokai Pang, Heming Zhu, Adam Kortylewski, Christian Theobalt, and Marc Habermann. 2024. ASH: Animatable Gaussian Splats for Efficient and Photoreal Human Rendering. In *IEEE/CVF Conference on Computer Vision and Pattern Recognition (CVPR)*.
- Jeong Joon Park, Pete Florence, Julian Straub, Richard Newcombe, and Steven Lovegrove. 2019. DeepSDF: Learning Continuous Signed Distance Functions for Shape Representation. *IEEE/CVF Conference on Computer Vision and Pattern Recognition (CVPR)* (2019).
- Georgios Pavlakos, Vasileios Choutas, Nima Ghorbani, Timo Bolkart, Ahmed A. A. Osman, Dimitrios Tzionas, and Michael J. Black. 2019. Expressive Body Capture: 3D Hands, Face, and Body from a Single Image. In *IEEE/CVF Conference on Computer Vision and Pattern Recognition (CVPR)*.
- Sida Peng, Junting Dong, Qianqian Wang, Shangzhan Zhang, Qing Shuai, Xiaowei Zhou, and Hujun Bao. 2021a. Animatable Neural Radiance Fields for Modeling Dynamic Human Bodies. In *IEEE International Conference on Computer Vision (ICCV)*.
- Sen Peng, Weixing Xie, Zilong Wang, Xiaohu Guo, Zhonggui Chen, Baorong Yang, and Xiao Dong. 2025. RMAvatar: Photorealistic human avatar reconstruction from monocular video based on rectified mesh-embedded Gaussians. *Graphical Models* 139 (2025).
- Sida Peng, Yuanqing Zhang, Yinghao Xu, Qianqian Wang, Qing Shuai, Hujun Bao, and Xiaowei Zhou. 2021b. Neural Body: Implicit Neural Representations With Structured Latent Codes for Novel View Synthesis of Dynamic Humans. In *IEEE/CVF Conference on Computer Vision and Pattern Recognition (CVPR)*.
- Zhiyi Qian, Shaofei Wang, Marko Mihajlovic, Andreas Geiger, and Siyu Tang. 2024. 3DGs-Avatar: Animatable Avatars via Deformable 3D Gaussian Splatting. In *IEEE/CVF Conference on Computer Vision and Pattern Recognition (CVPR)*.
- Shunsuke Saito, Jinlong Yang, Qianli Ma, and Michael J. Black. 2021. SCANimate: Weakly Supervised Learning of Skinned Clothed Avatar Networks. In *IEEE/CVF Conference on Computer Vision and Pattern Recognition (CVPR)*.
- Zhijiang Shao, Zhaolong Wang, Zhuang Li, Duotun Wang, Xiangru Lin, Yu Zhang, Mingming Fan, and Zeyu Wang. 2024. Splattingavatar: Realistic real-time human avatars with mesh-embedded gaussian splatting. In *IEEE/CVF Conference on Computer Vision and Pattern Recognition (CVPR)*.
- Shih-Yang Su, Frank Yu, Michael Zollhoefer, and Helge Rhodin. 2021. A-NeRF: Articulated Neural Radiance Fields for Learning Human Shape, Appearance, and Pose. In *Advanced Neural Information Processing Systems (NeurIPS)*, Vol. 34.
- Matthew Tancik, Pratul Srinivasan, Ben Mildenhall, Sara Fridovich-Keil, Nithin Raghavan, Utkarsh Singhal, Ravi Ramamoorthi, Jonathan Barron, and Ren Ng. 2020. Fourier Features Let Networks Learn High Frequency Functions in Low Dimensional Domains. *Advanced Neural Information Processing Systems (NeurIPS)* 33 (2020).
- Zhou Wang, Alan C Bovik, Hamid R Sheikh, and Eero P Simoncelli. 2004. Image quality assessment: from error visibility to structural similarity. *IEEE transactions on image processing* 13, 4 (2004), 600–612.
- Jing Wen, Xiaoming Zhao, Zhongzheng Ren, Alexander G. Schwing, and Shenlong Wang. 2024. GoMAvatar: Efficient Animatable Human Modeling from Monocular Video Using Gaussians-on-Mesh. In *IEEE/CVF Conference on Computer Vision and Pattern Recognition (CVPR)*.
- Chung-Yi Weng, Brian Curless, Pratul P. Srinivasan, Jonathan T. Barron, and Ira Kemelmacher-Shlizerman. 2022. HumanNeRF: Free-Viewpoint Rendering of Moving People From Monocular Video. In *IEEE/CVF Conference on Computer Vision and Pattern Recognition (CVPR)*.
- Hongyi Xu, Eduard Gabriel Bazavan, Andrei Zanfir, William T Freeman, Rahul Sukthankar, and Cristian Sminchisescu. 2020. GHUM & GHUML: Generative 3D Human Shape and Articulated Pose Models. In *IEEE/CVF Conference on Computer Vision and Pattern Recognition (CVPR)*.
- Zhengming Yu, Wei Cheng, Xian Liu, Wayne Wu, and Kwan-Yee Lin. 2023. Monohuman: Animatable human neural field from monocular video. In *IEEE/CVF Conference on Computer Vision and Pattern Recognition (CVPR)*.
- Ye Yuan, Xueting Li, Yangyi Huang, Shalini De Mello, Koki Nagano, Jan Kautz, and Umar Iqbal. 2024. Gavatar: Animatable 3d gaussian avatars with implicit mesh learning.

- In *IEEE/CVF Conference on Computer Vision and Pattern Recognition (CVPR)*.
- Youyi Zhan, Tianjia Shao, Yin Yang, and Kun Zhou. 2025. Real-time high-fidelity Gaussian human avatars with position-based interpolation of spatially distributed MLPs. In *IEEE/CVF Conference on Computer Vision and Pattern Recognition (CVPR)*.
- Jianfeng Zhang, Zihang Jiang, Dingdong Yang, Hongyi Xu, Yichun Shi, Guoxian Song, Zhongcong Xu, Xinchao Wang, and Jiashi Feng. 2022. Avatargen: a 3d generative model for animatable human avatars. In *European Conference on Computer Vision (ECCV)*.
- Richard Zhang, Phillip Isola, Alexei A. Efros, Eli Shechtman, and Oliver Wang. 2018. The Unreasonable Effectiveness of Deep Features as a Perceptual Metric. arXiv:1801.03924 [cs.CV] <https://arxiv.org/abs/1801.03924>
- Xuanmeng Zhang, Jianfeng Zhang, Rohan Chacko, Hongyi Xu, Guoxian Song, Yi Yang, and Jiashi Feng. 2023. Getavatar: Generative textured meshes for animatable human avatars. In *IEEE International Conference on Computer Vision (ICCV)*.
- Yiqun Zhao, Chenming Wu, Binbin Huang, Yihao Zhi, Chen Zhao, Jingdong Wang, and Shenghua Gao. 2025. Surfel-based Gaussian inverse rendering for fast and relightable dynamic human reconstruction from monocular videos. *IEEE Transactions on Pattern Analysis and Machine Intelligence (TPAMI)* (2025).
- Zerong Zheng, Han Huang, Tao Yu, Hongwen Zhang, Yandong Guo, and Yebin Liu. 2022a. Structured local radiance fields for human avatar modeling. In *IEEE/CVF Conference on Computer Vision and Pattern Recognition (CVPR)*.
- Zerong Zheng, Han Huang, Tao Yu, Hongwen Zhang, Yandong Guo, and Yebin Liu. 2022b. Structured Local Radiance Fields for Human Avatar Modeling. arXiv:2203.14478 [cs.CV] <https://arxiv.org/abs/2203.14478>